ELSEVIER

Journal of Structural Geology 26 (2004) 583–594

JOURNAL OF STRUCTURAL GEOLOGY

www.elsevier.com/locate/jsg

Implications of rapid, dike-fed pluton growth for host-rock strain rates and emplacement mechanisms

Christopher Gerbi[a,*], Scott E. Johnson[a], Scott R. Paterson[b]

[a]*Department of Geological Sciences, University of Maine, Orono, ME 04469-5790, USA*
[b]*Department of Earth Sciences, University of Southern California, Los Angeles, CA 90089-0740, USA*

Received 9 June 2002; received in revised form 1 August 2003; accepted 1 August 2003

Abstract

Dikes must maintain a critical width and flow velocity in order to propagate several kilometers from source to sink without freezing; consequently, they must support a high volumetric magma flow rate. This in turn implies that plutons fed by dikes must fill rapidly. In an effort to predict host-rock strain rates required by dike-fed growth, we employ a three-dimensional geometric model consisting of concentric shells to track instantaneous strain rates in a homogeneously deforming aureole around spheroidal plutons with a range of aspect ratios. Using published values for magma and host-rock parameters appropriate for mid-crustal levels, we calculate, for example, a minimum instantaneous strain rate of approximately 10^{-10} s^{-1} in the deformation aureole of a 1 km radius spherical pluton. Aureole strain rates, which range upward to greater than 10^{-4} s^{-1}, are primarily a function of position in the aureole, pluton size, and filling rate; pluton shape plays only a secondary role. Although preservation of evidence for high strain rates may be rare, and although multiple mechanisms probably operate simultaneously, we expect that deformation this rapid in the middle crust would be accommodated primarily by brittle mechanisms.

Keywords: Strain rate; Pluton emplacement; Magma transport; Microstructures

1. Introduction

Silicic magmatism plays a major role in crustal growth and evolution, but the relative importance of various mechanisms, such as diapirs and dikes, by which magma moves from its source region to a magma chamber remains unresolved (e.g. Clemens et al., 1997; Clemens, 1998; Miller and Paterson, 1999). Magma transport is only one of many mass transfer processes that operate within the crust, and the movement of molten material is intimately coupled to crustal rheology as well as strain and strain rate patterns both near and far from a pluton (Paterson and Fowler, 1993). Therefore, to evaluate the efficacy of different magma transport mechanisms, we must consider how the crust responds to the movement and collection of magma.

In recent years, attention has focused on dikes as an efficient method for rapidly moving large quantities of silicic magma through the crust. Some studies have considered the physical conditions required for fracture propagation (Clemens and Mawer, 1992; Rubin, 1995), whereas others have addressed questions related to the flow rate of magma through dikes (Bruce and Huppert, 1990; Petford, 1996; Petford et al., 2000). Despite some concerns about the likelihood of dike propagation (Rubin, 1995), these studies raise the possibility of generating a 6000 km^3 dike-fed mid-crustal pluton in less than 400 years (Petford et al., 1993). Although magma transport and emplacement have been considered somewhat independent processes (e.g. Clemens et al., 1997), some degree of in-situ expansion must accompany dike-fed pluton growth. To permit such growth, wall rocks must be able to deform sufficiently fast to accommodate the high volumetric fluxes associated with dikes. Addressing this point, Clemens et al. (1997, p. 157) stated that "Given the various forces applied to potential host rocks by the magma, spaces should be able to open relatively rapidly—so magma supply is most likely to provide the overriding rate-limit.". However, only a few studies have quantitatively evaluated the rates at which space-making mechanisms must operate. Some examples include those by Nyman et al. (1995), who inferred that the aureole around the Papoose Flat pluton deformed at a finite

* Corresponding author. Tel.: +1-207-581-2122; fax: +1-207-581-2202.
E-mail address: gerbi@umit.maine.edu (C. Gerbi).

0191-8141/$ - see front matter © 2003 Elsevier Ltd. All rights reserved.
doi:10.1016/j.jsg.2003.08.008

rate of approximately $10^{-12}\,s^{-1}$, and Fernandez and Castro (1999), who suggested rates as high as $10^{-10}\,s^{-1}$ in rocks surrounding parts of the Extremadura batholith. Using a geometrical approach, Johnson et al. (2001) calculated finite strain rates ranging upward from approximately $10^{-10}\,s^{-1}$, with the exact value depending on pluton size and filling rate.

To provide additional constraints on instantaneous strain rates associated with emplacement of silicic magma, we have constructed a three-dimensional geometrical model to evaluate the rates of homogeneous host-rock deformation during in-situ expansion of spheroidal dike-fed plutons. We use rock and magma parameters applicable to mid-crustal levels and a geometrical construction similar to that employed in other pluton aureole strain studies (e.g. Holder, 1979; Ramsay, 1989; Tikoff et al., 1999). Our results indicate that instantaneous strain rates fall in the range of $10^{-7.5}$–$10^{-11}\,s^{-1}$ for most rocks within the deformation aureole of a dike-fed pluton up to 5 km in radius. These strain rates are too fast to be measured with standard geochronological techniques, but host-rock microstructures may record strain rates of this magnitude. After presenting the model and the results, we discuss the microstructures likely to be indicative of these strain rates and assess the potential for their preservation. This study should not be construed either as supporting or disputing dike-fed pluton growth; our intention is to present some consequences of in-situ expansion of a dike-fed pluton.

2. Model parameters

2.1. Derivation of strain rate in the general spheroidal case

We use a three-dimensional, isovolumetric shell as the basis for calculating strain rates around an expanding pluton (Fig. 1). This geometrical model considers a spheroidal pluton fed by a dike of 1 km plan length. All near-field mass transfer accommodating the growing pluton occurs by homogeneous deformation in isotropic host rock. Around an expanding sphere, all deformation is symmetric and accomplished by coaxial deformation (Fig. 1a). In the general case, noncoaxial deformation occurs in most locations around an expanding spheroid, but for this work we have restricted our calculations to the loci of coaxial deformation along the principal axes of the spheroid (Fig. 1b). Our model does not explicitly incorporate surface uplift, far-field return flow to the source area, or discrete faults and shear zones.

As a model spheroidal pluton expands, a concentric shell with pre-pluton thickness τ^0 will thin to τ and increase its radius to maintain a constant volume (Fig. 1). In all expressions, the superscript 0 refers to the initial state. Because volume remains constant, shell thickness is coupled to the shell radius; this is the starting point for the following derivations using the instantaneous rate of thinning to calculate strain rate.

To determine the radius of the deforming shell, we must consider the original shell size and the added pluton volume. The original volume contained inside the shell is:

$$V_{in}^0 = \frac{4}{3}\pi r_{in}^{0^3} \tag{1}$$

where r_{in}^0 is the initial inner radius of the shell. With emplacement of a spheroidal pluton, the deforming shell will develop a spheroidal shape, but we always begin with a spherical shell because a spherical initial shell geometry is independent of the final pluton shape and thus allows comparisons between all models, and because we assume the host rock is isotropic and has no inherent shape-preferred structure. The volume inside the shell will change with the addition of a pluton by:

$$V_{in} = V_{in}^0 + V_p \tag{2}$$

where the subscript p refers to the pluton. In radius notation, the volume of the pluton and the volume inside the shell are (Fig. 1):

$$V_p = \frac{4}{3}\pi\alpha^2 r_p^3 \tag{3a}$$

$$V_{in} = \frac{4}{3}\pi(r_p + d_{in})(\alpha r_p + \gamma d_{in})^2 \tag{3b}$$

where d_{in} is the distance between the edge of the pluton and the inside of the shell, α is the pluton aspect ratio, defined as the ratio of the lengths of the horizontal to vertical axes of the spheroid; the two horizontal axes of the spheroid are equal. The shell thickness ratio, γ, allows for different degrees of shortening at the top and sides of the shell (Fig. 1b). We define the shell thickness ratio as:

$$\gamma = \frac{\tau_s}{\tau_t} \tag{4}$$

where the subscripts s and t refer to the side and top (or bottom) of the expanding pluton. Both α and γ, are imposed conditions, and we can assign them to be constant or vary with pluton radius. Substituting Eqs. (1), (3a) and (3b) into Eq. (2):

$$\frac{4}{3}\pi(r_p + d_{in})(\alpha r_p + \gamma d_{in})^2 = \frac{4}{3}\pi r_{in}^{0^3} + \frac{4}{3}\pi\alpha^2 r_p^3 \tag{5a}$$

The volume contained by the outer edge of the shell, d_{out}, follows similarly:

$$\frac{4}{3}\pi(r_p + d_{out})(\alpha r_p + \gamma d_{out})^2 = \frac{4}{3}\pi(r_{in}^0 + \tau^0)^3 + \frac{4}{3}\pi\alpha^2 r_p^3 \tag{5b}$$

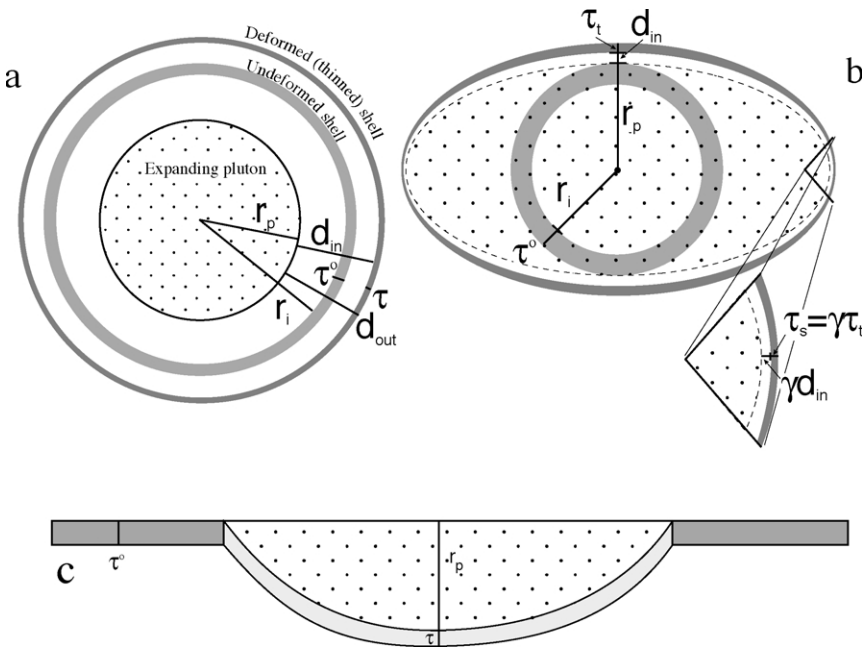

Fig. 1. Vertical central cross-sections illustrating the geometric bases for models of an in-situ expanding spheroidal pluton. See text for explanation of variables. (a) As a spherical pluton expands from a point source, a spherical shell of wall rocks deforms symmetrically, expanding and thinning. Light gray represents the initial, undeformed shell; the dark gray shell corresponds to the instance where a pluton of radius r_p has intruded. (b) In the more general case of a spheroidal pluton, the deforming shell has either a uniform thickness, or thins more at the ends. We define the shell thickness ratio, $\gamma = \tau_s/\tau_t$. This ratio also applies to the distance between the pluton and the shell of interest (d_{in}). (c) A pluton inflating from a sill to a hemisphere by floor subsidence drives uniform thinning of model host-rock layer (light gray) beneath the expanding pluton with a fixed horizontal dimension. This geometry also applies, if inverted, to a laccolith geometry.

We define the shell thickness as (Fig. 1):

$$\tau = d_{out} - d_{in} \tag{6}$$

Solving Eqs. (5a) and (5b) for d_{in} and d_{out} allows us to calculate τ as a function of r_p (see Appendix A). The strain rate related to the thinning shell, $d\tau/dt$ (derived below), is thus a function of the change in pluton radius with respect to time.

The derivative of Eq. (3a) with respect to r_p, recalling that α is either constant or a function of r_p, is:

$$\frac{dV_p}{dr_p} = \left(4\pi\alpha^2 r_p^2\right) + \frac{8}{3}\pi\alpha r_p^3 \frac{d\alpha}{dr_p} \tag{7a}$$

The volume rate of change of the pluton is equivalent to the filling rate, Q:

$$\frac{dV_p}{dt} = Q \tag{7b}$$

Combining Eqs. (7a) and (7b):

$$\frac{dr_p}{dt} = \frac{dr_p}{dV_p}\frac{dV_p}{dt} = \frac{Q}{\left(4\pi\alpha^2 r_p^2\right) + \frac{8}{3}\pi\alpha r_p^3 \frac{d\alpha}{dr_p}} \tag{7c}$$

Multiplying the derivative of τ with respect to r_p by Eq. (7c) yields:

$$\frac{d\tau}{dr_p}\frac{dr_p}{dt} = \frac{d\tau}{dt} \tag{8}$$

The instantaneous strain rate for a deforming shell is then:

$$\dot{\epsilon} = \frac{(d\tau/dt)}{\tau} \tag{9}$$

2.2. Floor subsidence and roof doming

To consider the possibility that a pluton may grow by inflation from a sill into a laccolith or lopolith geometry by roof doming (Corry, 1988; Morgan et al., 1998) or floor subsidence (Cruden, 1998; Wiebe and Collins, 1998; Cruden and McCaffrey, 2001), we constructed another model geometry using a constant horizontal width. To do so, we constantly change the aspect ratio as the pluton expands. The final geometry of this model is a hemisphere with a 5 km radius (Fig. 1c). As the circumference of the pluton increases, the shells in this model stretch uniformly either underneath the deforming floor, as shown in Fig. 1c, or over the roof of the pluton. Because we assume that no surface uplift occurs, roof doming is mathematically equivalent to floor subsidence.

2.3. Filling rate

The strain rate in our model depends strongly on the pluton filling rate, or the magma flux through the feeder dike. We calculated the volumetric flux through a single dike using published values for the various parameters that determine critical dike widths and flow rates (Bruce and Huppert, 1990; Petford et al., 1993; Clemens et al., 1997; Cruden, 1998). The magmatic flux, Q, is the product of the dike width, flow rate, and plan length. We use a dike plan length of 1 km. The critical width, w, necessary to prevent a dike from freezing depends on the viscosity, η, thermal diffusivity, κ, density contrast between the magma and host rock, $\Delta\rho$, acceleration due to gravity, g, latent heat of solidification, L, specific heat, C, vertical dike length, H, initial magma temperature, T_m, effective magma freezing temperature, T_w, and far field temperature of the host rock, T_∞ (Bruce and Huppert, 1990; Petford et al., 1993):

$$w = 1.5\left(\frac{C(T_w - T_\infty)^2}{L(T_m - T_w)}\right)^{\frac{3}{4}}\left(\frac{\eta\kappa H}{g\Delta\rho}\right)^{\frac{1}{4}} \quad (10)$$

Using the width from Eq. (10), the velocity, v, assuming buoyancy-driven flow, is:

$$v = \frac{g\Delta\rho w^2}{12\eta} \quad (11)$$

Using a range of physical magma parameters suggested by Clemens and Petford (1999), we calculated a range of volumetric flow rates of 5.62–179 m^3/s (Table 1). These flow rates are based on a mid-crustal emplacement level (far-field temperature of 450 °C). The slow rate is for a relatively dry tonalite melt with viscosity of 10^7 Pa s, initial temperature of 950 °C, and density difference between host rock and magma of 200 kg/m^3. The fast rate is for a wet granitic melt with viscosity of 10^4 Pa s, initial temperature of 850 °C, and density difference between host rock and magma of 400 kg/m^3. Other combinations of viscosity, magma temperature, and density difference between the above values yield intermediate volumetric flow rates. These flow rates are for dikes at the critical, or minimum, width to prevent freezing; dikes could be wider and therefore have higher flow rates. Thus, given the above conditions, we regard the flow rate of 5.62 m^3/s as the minimum filling rate for a pluton fed by a dike 1 km in plan length.

Table 1
Magma parameters and calculated volumetric flow rates in dikes

Constants		
Thermal diffusivity, κ (m^2/s)	8×10^{-7}	
Latent heat of solidification, L (J/kg)	3×10^5	
Specific heat, C (J/kg/°C)	1.2×10^3	
Acceleration due to gravity, g (m/s^2)	9.8	
Vertical dike length, H (m)	2×10^4	
Effective magma freezing temperature, T_w (°C)	750	
Horizontal dike length (m)	10^3	
Far field host rock temperature, T_∞ (°C)	450	
Variables	For low flux	For high flux
Initial magma temperature, T_m (°C)	950	850
Density contrast, $\Delta\rho$ (kg/m^3)	200	400
Viscosity, η (Pa s)	10^7	10^4
Output		
Dike width, w (m)	7.01	1.76
Magma velocity, v (m/s)	0.0008	0.101
Volumetric flux, Q (m^3/s)	5.62	179

Input values, except horizontal dike length, from the range of permissible values given by Bruce and Huppert (1990), Petford et al. (1993), and Clemens and Petford (1999).

The geometry of our model does not explicitly assume a mid-crustal pluton emplacement level. However, because the parameters we used to calculate magma flow rates are based on values most consistent with the middle crust, the strain rates we derive are most applicable to those levels. Higher temperatures deeper in the crust reduce the critical magma flow rate, perhaps to approximately 10^{-5} m^3/s. At such low flow rates, a pluton should expand much more slowly and require much lower host-rock strain rates.

3. Results

To evaluate the host-rock strain-rates associated with a range of pluton growth histories, we employed various values for filling rate, pluton aspect ratio, and shell thickness ratio (Table 2). Filling rates were 5.62 and 179 m^3/s, and pluton aspect ratios were 1, 2, 5, and a size-dependent function calculated from McCaffrey and Petford (1997):

$$\alpha = 2.34 r_p^{1.67} \quad (12)$$

where r_p is the vertical pluton radius. All shells initially have a uniform thickness ($\gamma = 1$), so for a different shell thickness ratio to develop after a pluton grows, the shell thickness ratio must vary with r_p. For those cases, we chose functions (Table 2) so that the ratio between the thickness at the side and at the top of the shell was approximately 0.5 at the end of the model run. The ratio of 0.5 is an arbitrary value, but represents a reasonable estimate of differential strain around a pluton. In all model runs, strain rates in shells surrounding an expanding pluton decrease monotonically with both r_p and distance from the pluton (Figs. 2 and 3a). Additional runs, not described here, indicated that results were not sensitive to initial shell thickness, so for all the runs we discuss, the initial shell thickness is 1 m. We chose the plan length of 1 km as a reasonable estimate for dikes feeding plutons on the order of 5 km in radius. As shown by Johnson et al. (2001), a different plan length, even

Table 2
Parameters for model runs

Run[a]	Magma flux Q (m^3/s)	Initial inner shell radius r_i (m)	Pluton aspect ratio α_p	Shell thickness ratio γ	Vertical pluton radius r_p (m)	Initial shell thickness Δr (m)
1	5.62	0	1	1	–	1
2	5.62	1000	1	1	–	1
3	179	0	1	1	–	1
4	179	1000	1	1	–	1
5	5.62	500	2	1	–	1
6	5.62	500	5	1	–	1
7	5.62	500	$2.34r_p^{5/3}$[b]	1	–	1
8	5.62	500	5	$-0.5(r_p/1000)^2+1$	–	1
9	5.62	–	1	1	1000	1
10	179	–	1	1	1000	1
11	5.62	–	5	$-0.5(r_p/1000)^2+1$	200	1
12[c]	5.62	500	$5/r_p$	1	–	1
13[c]	179	500	$5/r_p$	1	–	1

[a] For runs 1–8, see Fig. 2; for 9–11, see Fig. 3.
[b] Calculated from McCaffrey and Petford (1997).
[c] Models a pluton with a constant 5 km radius inflating from a sill (see Fig. 4).

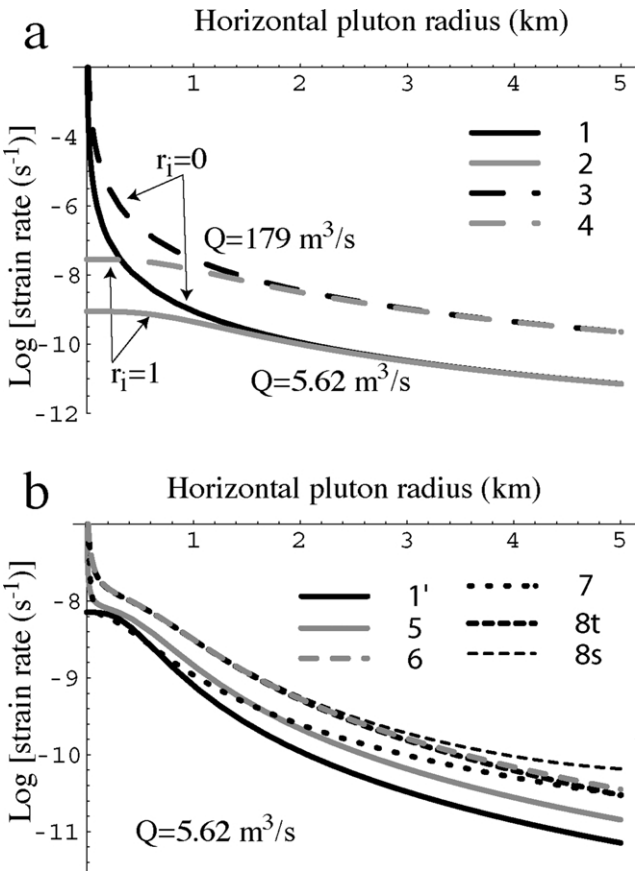

Fig. 2. (a) Results from model runs 1–4 (legend refers to Table 2), showing dependence of strain rate on initial shell radius (r_i) and on filling rate (Q). (b) Results from runs 5–8 (Table 2) and from a run with a sphere for comparison (labeled 1′: parameters as run 1 (Table 2) except that $r_i = 500$ m for comparison with runs 5–8). Postscripts t and s refer to top and side, respectively, of the deforming shell (Fig. 1b). Runs 5–8, which are based on the minimum filling rate, represent the lowest predicted strain rates for dike-fed pluton expanding in-situ.

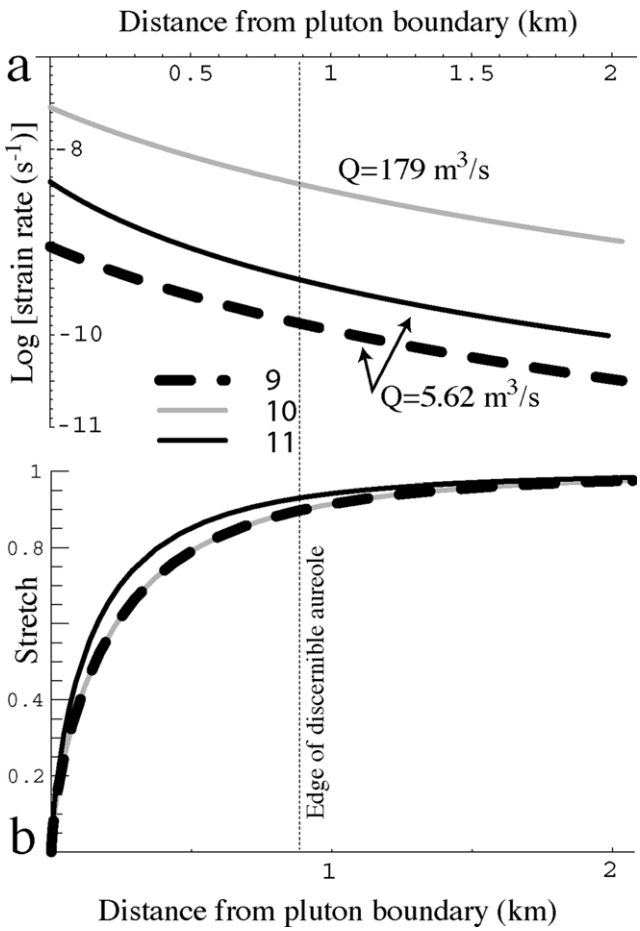

Fig. 3. Results of model runs 9–11 (Table 2). (a) Snapshot of horizontal instantaneous strain rates and stretch distributions across deformation aureoles surrounding a 1 km horizontal radius pluton. (b) The finite strain gradient, shown as the change in stretch (ratio of final to initial length) with distance from the edge of the pluton. We arbitrarily define the edge of the aureole as the locus of 10% shortening, or stretch of 0.9, which occurs at approximately one pluton radius from the pluton boundary.

one that grows as the pluton expands, has little effect on the modeled strain rates.

3.1. Range of permissible strain rates

Around a 1 km pluton, rocks in the aureole deform at rates higher than $10^{-10}\,s^{-1}$ (Figs. 2 and 3). Considering all modeled geometries and different observation positions in the aureole, we calculate instantaneous strain rates that range from $10^{-11}\,s^{-1}$ to greater than $10^{-4}\,s^{-1}$. The calculated strain rates depend primarily on the size of the pluton, the original shell distance from the pluton center (i.e. where in the aureole the strain rate is measured), and the filling rate, such that greater distance from the pluton contact, larger pluton radius, and lower dike flow rate contribute to lower strain rates. A uniform shell thickness around a spherical pluton (Fig. 2b, Run 1′) produces lower strain rates than other geometries, but the effect of pluton shape and deformation shell uniformity is of secondary importance (Fig. 2b).

As a pluton expands at a constant volumetric rate, the instantaneous strain rate everywhere in the aureole diminishes (Fig. 2), with the very high rates for rocks adjacent to the pluton boundary decaying rapidly (Fig. 2a). As an example, a shell that started 1 km from the center of a spherical pluton 1 km in radius deforms at $10^{-7.5}$–$10^{-9}\,s^{-1}$, depending on filling rate (Fig. 2a). As the pluton grows to 5 km radius, the strain rates decrease to a range of $10^{-9.5}$–$10^{-11}\,s^{-1}$. Results are similar for the non-spherical cases. Except during the earliest stages of growth ($r_p < \sim 750$ m), the instantaneous strain rate varies less than an order of magnitude across the aureole (Figs. 2a and 3).

For the floor subsidence and roof doming model, strain rates are nearly constant, decreasing by less than an order of magnitude as the pluton inflates (Fig. 4). Recall that this strain rate measures the thinning of a shell under a sinking floor or over a doming roof, and does not incorporate any lateral expansion; the pluton is assumed to inflate vertically from a sill. As in the original model, strain rates are highly sensitive to filling rate, being approximately $10^{-9.3}$–$10^{-10.8}\,s^{-1}$ for the fast and slow filling rates, respectively. These rates are initially lower than those for the expanding spheroid (Fig. 2), but become equal or higher as the pluton grows.

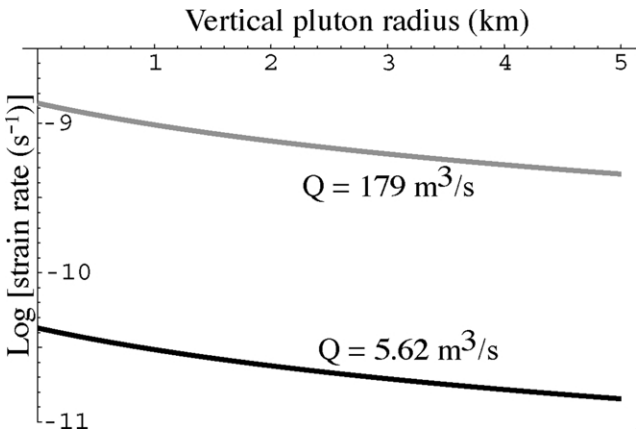

Fig. 4. Results of model runs 12 and 13 (Table 2): instantaneous strain rates associated with floor subsidence or roof doming around a spheroidal pluton with a constant horizontal radius of 5 km as it inflates from a sill. Initial shell radius is 500 m.

3.2. Effect of varying initial shell radius

The initial shell radius, or the distance a shell originated from the incipient pluton center, strongly affects the calculated strain and strain rate (Fig. 2), but it does not affect the strain or strain-rate fields. In effect, the initial shell radius identifies which shell we track through the model: a shell with initial radius of 0 km (Runs 1 and 3; Fig. 2a) represents the rocks at the pluton margin, whereas a shell with initial radius of 1 km (Runs 2 and 4; Fig. 2a) represents rocks that started 1 km from the pluton center. Because of thinning and translation associated with pluton growth, rocks that began 1 km from the pluton center end up 1.261 km from the center, and only 261 m from the boundary, of a 1 km radius pluton. Shells closer to the pluton center (lower r_i) predictably experience a higher initial strain rate as they rapidly thin to accommodate the growing pluton (Runs 1 and 3; Fig. 2a). However, shells starting at $r_i = 0$ and $r_i = 1$ km will experience different strain rates only until the pluton is approximately 1 km in radius (Fig. 2a). Intermediate values of r_i contour smoothly between these curves. To allow comparison among other variables, we discuss our remaining results for a shell that started 500 m from the pluton center.

3.3. Effect of varying filling rate

Wall-rock strain rate is highly sensitive to the pluton filling rate. The filling rates used here are based on theoretical and experimental determinations of magma characteristics and flow dynamics (Bruce and Huppert, 1990; Petford et al., 1993; Clemens et al., 1997; Cruden, 1998) relevant to mid-crustal levels. Rocks surrounding a pluton filling at the lower end of the flux range will experience strain rates nearly 1.5 orders of magnitude lower than those around a pluton filling at the higher rate (Fig. 2a). Because the difference between the minimum and maximum filling rates is also approximately 1.5 orders of magnitude, we can consider the strain rate to scale approximately linearly with the filling rate.

3.4. Effect of varying aspect ratio and shell thickness ratio

Compared with a uniform shell thickness surrounding a spherical pluton, shell thickness ratio, γ, and pluton aspect ratio, α, have less than an order of magnitude effect on the

strain rate (Table 2; Figs. 2b and 3a). Similarly, the difference in strain rate at the top and sides of a non-spherical pluton is less than an order of magnitude (Runs 8s and 8t; Fig. 2b). Because we model the non-spherical plutons as oblate bodies, the sides of those plutons always experience strain rates greater than the top for a shell thickness ratio.

4. Corollary calculations

4.1. Stoping

Stoping has long been recognized as an efficient mechanism for removing inner portions of a deformation aureole (Buddington, 1959; Paterson et al., 1996). With that in mind, we modified our model to determine the effects of stoping on the instantaneous strain rate and finite strain distribution around a pluton with aspect ratios of 1 and 2, and consisting of 0, 20, and 50% stoped blocks by volume. In this model, stoping is assumed to operate uniformly around the spheroidal pluton (Fig. 5a). The fundamental difference between this model and those previously described is that the pluton radius includes volume of both the magma added and the stoped blocks. Because stoped blocks constitute a portion of the pluton, the *effective* pluton radius for a given volume of dike-fed magma is larger than it would be without stoping (Fig. 5b).

Because the response of the rocks outside the effective radius of the pluton depends only on the volume added to the system (Eq. (2)), the degree of stoping does not influence deformation of rocks in the aureole. Although strain rate and finite strain distributions around plutons with stoped material (Fig. 5c and d) appear to be sensitive to the degree of stoping when viewed in relation to the *edge* of the pluton, if the same strain-rate curves are plotted in relation to the *center* of the pluton, they are identical. Therefore we expect that, given the same volumetric magma flux, aureoles around plutons with high degrees of stoping deform at strain rates equivalent to those around plutons with no stoping.

Although it does not significantly affect predicted strain rates, stoping does affect the finite strain distribution in the aureole. In particular, because the pluton has incorporated the inner, high-strain portion of the aureole, rocks adjacent to the pluton have a lower finite strain with increased degree of stoping (Fig. 5d; Table 3). This in turn affects the bulk

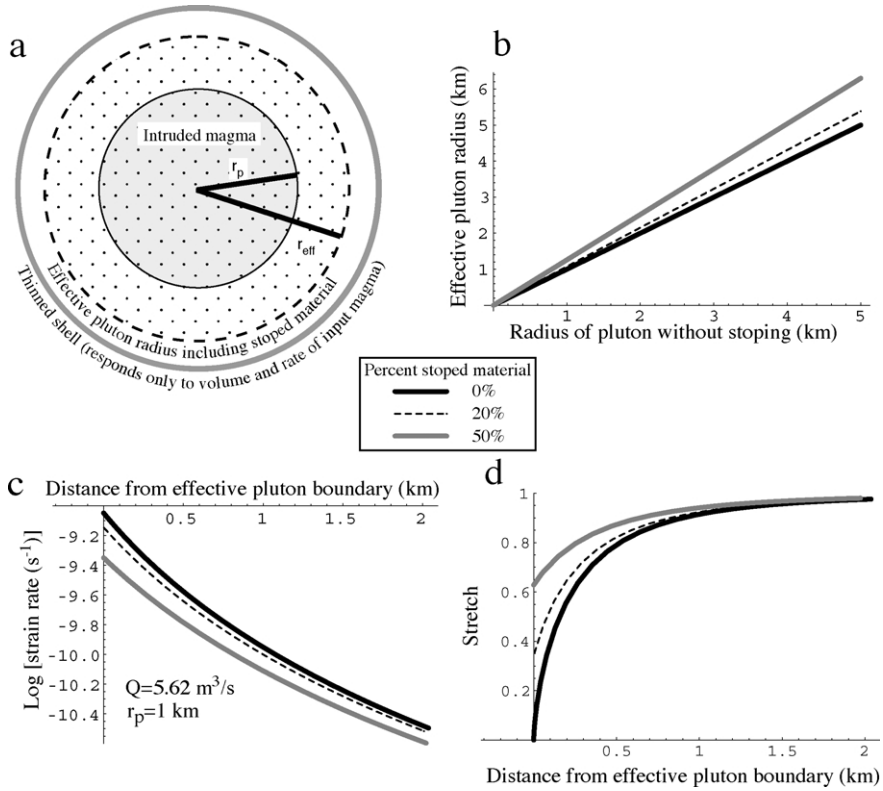

Fig. 5. (a) Central cross-section of a spherical pluton that incorporates stoped blocks. If some fraction of the pluton consists of stoped material, the effective pluton radius, r_{eff}, will be larger than the pluton radius, r_p, to which the deforming shells are responding. Stoping removes the high strain portion of the inner aureole and decreases the bulk strain across the remainder of the aureole. For clarity, the undeformed shell is not shown, but it is the same as in Fig. 1a. (b) Relationship between the effective pluton radius and the radius of the emplaced magma (not including stoped blocks), which we model as a sphere at the center of the pluton. (c) Instantaneous strain rate distribution, for different degrees of stoping, across the deformation aureole surrounding a 1 km radius pluton filled at the minimum rate. (d) Stretch distribution, for different degrees of stoping, across the deformation aureole surrounding a 1 km radius pluton. Because stoping uniformly removes the high strain inner portion of the aureole, with higher degrees of stoping, rocks immediately adjacent to the effective pluton boundary are less strained.

Table 3
Strain-related calculations for different degrees of stoping

Stoping (% total pluton volume)	Pluton aspect ratio	Aureole width normalized to pluton radius	Horizontal radial accommodation[a] (%)	Maximum shortening (at pluton margin) (%)
0	1	0.9	90	>99
20	1	0.76	32	66
50	1	0.50	13	37
0	2	0.75	74	>99
20	2	0.63	30	68
50	2	0.39	17	39

[a] Percentage of pluton radius accommodated by bulk shortening across the aureole.

strain of the aureole. If we define the edge of the deformation aureole at 10% shortening, equivalent to a stretch of 0.9, and consider a central section through a spherical pluton, we can calculate, for different degrees of stoping, the aureole width normalized to the pluton radius and the percentage of the pluton radius accounted for by the linear shortening in the aureole (Table 3). Normalized aureole widths range from 0.9 for no stoping and an aspect ratio of 1, to 0.39 for 50% stoping and an aspect ratio of 2. Homogeneous shortening accounts for only 32 and 13% of the pluton radius at 20 and 50% stoping, respectively, as compared with 90% with no stoping. The maximum observable shortening at the pluton boundary around spherical plutons with 20 and 50% stoping are 66 and 37%, respectively. The modeled aureole widths and radial accommodation values incorporating stoping are in agreement with those determined by Paterson and Fowler (1993) for six natural plutons.

4.2. Tectonic accommodation

Based on field mapping and analog modeling, several studies have proposed dilational sites associated with faults, such as those in pull-apart basins or along normal faults, as locations where plutons can develop (e.g. Hutton, 1982; Guineberteau et al., 1987; Hutton, 1988b; Tikoff and Teyssier, 1992; Ferre et al., 1995; Benn et al., 1998). For this mechanism to accommodate an inflating pluton, the dilation rate must at least equal the rate at which the walls of the pluton diverge (twice the rate at which the pluton radius grows). The pluton radial growth rate depends on the magmatic flux and pluton geometry. We can use Eq. (7c) to calculate those rates for a central section of a spherical pluton:

$$2\frac{\mathrm{d}r_\mathrm{p}}{\mathrm{d}t} = 2\frac{Q}{4\pi r_\mathrm{p}^2} = \frac{Q}{2\pi r_\mathrm{p}^2} \tag{13}$$

Around a 1 km radius pluton filled at the slowest permissible rate (Table 1), the host-rock walls must diverge at approximately 28 m/yr (Fig. 6), faster than the rate calculated by Fernandez and Castro (1999) for a pluton in the Central Extremadura batholith. Plutons growing in pull-apart basins would probably have an aspect ratio closer to 2, but oriented so the short axis is horizontal and the two long axes lie in the vertical fault plane. Walls around the short axis of such a spheroid will diverge one quarter as fast as in the spherical case.

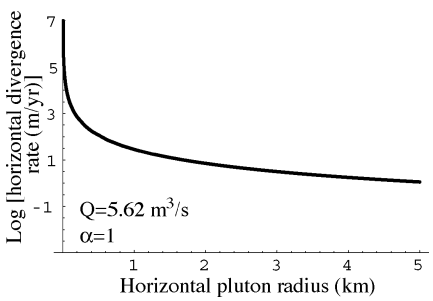

Fig. 6. Horizontal divergence rates of wall rocks necessary to accommodate the central section of a spherically expanding pluton fed by a dike with our minimum filling rate. Based on the geometries we have described, this curve represents the minimum divergence rate for the walls around the center of a spherical dike-fed pluton.

5. Discussion

5.1. Accommodating predicted strain rates

Although near-field and far-field material transfer processes together accommodate magma transfer (e.g. Hutton, 1988a; Paterson and Fowler, 1993), we have modeled only the near-field effects of a single intrusion driving homogeneous deformation in the host rock. Other near-field processes that may make space for magma, including regional tectonic strain, roof uplift, and floor subsidence, must also occur at rates sufficient to allow pluton growth in accordance with proposed filling rates (Paterson and Fowler, 1993; Cruden and McCaffrey, 2001). Below, we address the likelihood that these mechanisms can operate at sufficient rates to accommodate dike-fed pluton growth. Host-rock volume loss is another proposed space-making mechanism, but it is likely to be too slow to be significant at these strain rates (e.g. Marsh, 1989; Yoshinobu and Girty, 1999). As shown in Section 4.1, stoping does not

affect the strain rates in the aureole, so we do not discuss that mechanism further here.

5.1.1. Regional tectonic accommodation

Rates of bulk regional deformation are usually quoted in the range of 10^{-13}–10^{-15} s^{-1} (Pfiffner and Ramsay, 1982; Paterson and Tobisch, 1992; Dunlap et al., 1997; Foster and Gray, 1999; Muller et al., 2000). Although some workers have proposed that discrete zones, such as kink folds and shear zones, within tectonically active areas can deform much faster than the regional strain rate, strain rates at these local sites are suggested to be no greater than 10^{-9} s^{-1} (e.g. Schmid, 1989; White and Mawer, 1992; Fernandez and Castro, 1999). In some instances, it appears that shear zones or kink folds may deform fast enough to accommodate strain rates required by dike-fed pluton expansion, but shear strain rates associated with shear zones are not directly comparable with strain rates predicted by our model.

Perhaps a better measure for the ability of regional tectonic activity to make space for plutons would be the divergence rate of faults, such as in pull-apart basins. Divergent plate boundaries probably set the upper limit for making space by faulting (Paterson and Tobisch, 1992), with part of the East Pacific rise recognized as the fastest spreading center at 0.15 m/yr (Hey et al., 1995). This rate is two orders of magnitude lower than around the slowest-growing modeled spherical pluton (Section 4.2), much too slow to accommodate a pluton inflating in a single pulse at the lowest calculated filling rate.

5.1.2. Translation and rotation

Several recent models and interpretations of natural plutons have invoked variations of translation and rotation as accommodation mechanisms for expanding plutons (e.g. Cruden, 1998; Morgan et al., 1998; Wiebe and Collins, 1998; Tikoff et al., 1999; Cruden and McCaffrey, 2001). Without significant strain in the host rocks, translation and rotation must result in surface uplift, Moho depression, far-field plastic or brittle deformation, or downward transfer of material to the depleted pluton source (Paterson and Fowler, 1993). Surface uplift has been documented for plutons and laccoliths in the upper crust (e.g. Acocella and Mulugeta, 2001) and postulated for those in the middle crust (de Saint-Blanquat et al., 2001). Brown and McClelland (2000) suggested that Moho depression accommodated magmatic growth in the Coast Plutonic Complex.

Translation accompanying a penetratively thinning shell can be an accommodating factor (Tikoff et al., 1999), but rocks within and outside that shell must deform at high instantaneous strain rates ($>10^{-10}$ s^{-1}) during at least early stages of the deformation. In general, however, translation and rotation by themselves do not involve penetrative deformation, so structures at the boundaries of translating and rotating blocks must accumulate strain. In order to accommodate our modeled 1 km radius spherical pluton, translation or rotation must open space at a rate of at least 28 m/yr. This requires that rocks in zones bounding areas of rotation or translation must deform at equivalently high strain rates. Cruden (1998) has suggested that shear zones bounding a subsiding pluton floor (or a doming roof) must deform at shear strain rates greater than 10^{-10} s^{-1}.

5.2. Applying the model to natural settings

Our model uses a simple geometry to predict instantaneous strain rates in the deformation aureole of a spheroidal pluton as it expands concentrically in a single pulse. As such, it falls short of describing many naturally occurring plutons. Nevertheless, several studies, including reinterpretations of well-studied plutons, have argued for some degree of in-situ expansion during emplacement (e.g. Papoose Flat (Morgan et al., 1998), Flamanville (Brun et al., 1990), Ardara (Molyneux and Hutton, 2000), San José (Johnson et al., 2003a)). The composition and size of the Flamanville, San José, and Ardara plutons are appropriate for our model. If the in-situ expansion of these plutons was driven by an influx of dike-fed magma, the surrounding deformation may preserve microstructural evidence (see below) of instantaneous strain rates within the range suggested by our results.

5.2.1. Pluton evolution and episodic construction

Regardless of how a long-lived plutonic magma chamber eventually grows, it must initiate with a critical volume to prevent freezing. A smaller initial volume of magma is necessary in warmer host rock, as could develop if the host rock were preheated by a series of intrusions. If a pluton were fed by small, temporally spaced dike-fed injections, early injections would cool below their solidus before the next injection occurred, likely resulting in a sheeted complex, at least on the margins (Yoshinobu et al., 1998). Therefore, unless stoping or remelting removed the evidence, plutons with no sheeted margins probably originated as a substantial pulse of magma, whether or not they continued to grow episodically.

For plutons growing episodically, even though a single filling event may be fast, the long-term average magma supply rate can be low due to the time interval between injections. In an ideal system, the non-elastic host-rock strain rates during each filling event should be a function of the pluton size, shape, and filling rate, and thus be predicted by our model. Natural systems, however, may vary from the ideal in several important ways. For example, if hundreds of small injections intrude a large chamber (such as in the mafic–silic systems described by Wiebe and Collins (1998)), the host rock may have the capacity to absorb the additional volume elastically, or the small strains could be taken up by episodic faulting. Alternatively, magma entering the chamber from the bottom could induce an eruption or transfer of magma to a higher level chamber, thereby keeping the pluton volume approximately constant and eliminating any need for host-rock strain.

Some plutons that grow episodically do so with the

intrusion of only a few discrete pulses. Johnson et al. (2003, 2004) described a multiple pulse tonalite pluton in the Peninsular Ranges of Mexico. The initial pulse of this pluton apparently had time to undergo extensive crystallization at its margins before being intruded by a second pulse of tonalite magma. The partly crystallized outer shell of the pluton was deformed, at rates estimated by Johnson et al. (2004) to lie between approximately 10^{-8} and $10^{-11}\,s^{-1}$, during the emplacement of the second pulse. The partly crystallized carapace behaved mechanically as part of the host rock into which the magma intruded, so our model may be applicable to this type of system.

5.2.2. Field and microstructural evidence for high instantaneous strain rates

Obtaining strain-rate information from pluton aureoles is difficult, owing principally to the poor calibration of structures and microstructures to the dominantly transient thermal and dynamic conditions that existed in these environments. But under certain conditions, aureole rocks can record and retain evidence for high strain rates. Our above modeled strain rates are based on pluton filling rates calculated for a background temperature of 450 °C, and although not part of the calculations, this temperature might reasonably correspond to the upper middle crust, depending on geothermal gradients. Under these conditions, rocks straining at rates in excess of $10^{-10}\,s^{-1}$ are unlikely to flow, at least initially, by dislocation or diffusion creep processes. Therefore, around rapidly-filling plutons, we might expect widespread evidence for grain-scale brittle deformation regardless of the dominant mineralogy. In addition, the following observations are compatible with high strain rates (Johnson et al., 1999):

1. Brittle features such as radiating fracture sets oriented perpendicular to the direction of minimum compressive stress, local or extensive zones of brecciation, and extensive fracturing of minerals that were present prior to emplacement may be common. Gradients in the development of these features may be present, with the most intense development near the pluton margin.
2. Contact metamorphism will completely postdate the emplacement-related deformation, owing to the slow rate of heat transfer relative to the rate of pluton growth.
3. Synplutonic dikes may be isoclinally folded in the magmatic state prior to cooling below their solidus temperature.

At background temperatures higher than those used in our model, creep mechanisms may play an active role in accommodating deformation, but at mid-crustal levels, creep will not be a dominant mechanism (Albertz et al., 2002). The minimum strain rate we would predict at elevated background temperature would necessarily be lower because the minimum filling rate would be lower. In the early stages of pluton grown, however, strain rates would still be well above $10^{-10}\,s^{-1}$. Where creep is active, it may be possible to use experimentally derived flow laws to evaluate aureole strain rates. The principal difficulty with this approach is extrapolating experimental results, on either mono- or polymineralic rocks, to an environment where steady state thermal and dynamic conditions almost certainly never prevailed. Because strong and weak minerals will partition the strain and strain rate (e.g. Bons and Cox, 1994; Goodwin and Tikoff, 2002; Ji and Xia, 2002; Johnson et al., 2004), microstructures of the entire rock would have to be characterized in any attempt to determine the bulk strain rate.

Preservation of microstructures diagnostic of high strain rates in a pluton aureole requires certain conditions. If the pluton is large, with a large associated thermal flux into the aureole, evidence for microfracturing may be destroyed by recrystallization. Similarly, if the pluton is 'syntectonic', then continued accumulation of regional strain and associated differential stress may also affect the emplacement related microstructures. In general, the preservation of syn-emplacement microstructures would be favored by a rapid drop in temperature, differential stress and strain rate after emplacement (e.g. Knipe, 1989; Prior et al., 1990; White and Mawer, 1992; Handy et al., 2001; Johnson et al., 2004). These conditions are probably best met around relatively small post-tectonic plutons (e.g. radius <5 km) that formed from a single 'pulse' of magma.

6. Conclusion

Our three-dimensional model of homogeneous deformation in host rocks surrounding dike-fed, in-situ expanding plutons predicts, for example, instantaneous strain rates greater than $10^{-10}\,s^{-1}$ in the deformational aureole of a 1 km radius pluton. If all deformation is homogeneous, whether brittle or plastic, structures within the aureole should reflect those strain rates. With the operation of other material transfer processes, such as rigid block translation and rotation, structures bounding the blocks must themselves accommodate deformation at comparably high strain rates. Microstructures provide the best opportunity to record strain rates of this magnitude, provided they are not overprinted by later thermal or deformational events. The presence of evidence for high strain rates in deformation aureoles, whether the deformation is penetrative or in discrete zones, would be consistent with in-situ dike-fed pluton expansion as a magma emplacement mechanism.

Acknowledgements

We gratefully acknowledge support from an NSF Graduate Research Fellowship to C.G. and NSF Grant EAR-0087661 to S.E.J. Discussions with Terry Hughes clarified the mathematics, and constructive reviews from Brett Davis, Keith Klepeis, and Basil Tikoff strengthened the manuscript. We thank Joao Hippert for editorial assistance.

Appendix A

We derived the function relating the shell thickness to the pluton radius using the *Solve* function in Mathematica 4.0, by Wolfram Research, Inc. The explicit solution for shell thickness, τ, determined by solving Eqs. (5a) and (5b) for d_{in} and d_{out} and substituting the results into Eq. (6), is:

$$\tau = \frac{1}{2^{\frac{2}{3}}3\gamma^2} \times \left(\frac{-2r_p^2\gamma^2(\alpha-\gamma)^2}{\left(2\alpha^3\gamma^3r_p^3 + 27\gamma^4r_i^3 + 21\alpha^2\gamma^4r_p^3 + 6\alpha\gamma^5r_p^3 - 2\gamma^6r_p^3 + 3\sqrt{3(\gamma^7(r_i^3+\alpha^2r_p^3)(4\alpha^3r_p^3+27\gamma r_i^3+15\alpha^2r_p^3+12\alpha\gamma^2r_p^3-4\gamma^3r_p^3))}\right)^{\frac{1}{3}}} - \right.$$

$$\left(4\alpha^3\gamma^3r_p^3 + 54\gamma^4r_i^3 + 42\alpha^2\gamma^4r_p^3 + 12\alpha\gamma^5r_p^3 - 4\gamma^6r_p^3 + 6\sqrt{3(\gamma^7(r_i^3+\alpha^2r_p^3)(4\alpha^3r_p^3+27\gamma r_i^3+15\alpha^2r_p^3+12\alpha\gamma^2r_p^3-4\gamma^3r_p^3))}\right)^{\frac{1}{3}} +$$

$$\frac{-2r_p^2\gamma^2(\alpha-\gamma)^2}{\left(2\alpha^3\gamma^3r_p^3 + 27\gamma^4(r_i+\tau^0)^3 + 21\alpha^2\gamma^4r_p^3 + 6\alpha\gamma^5r_p^3 - 2\gamma^6r_p^3 + \sqrt{(\gamma^6(-4r_p^6(\alpha-\gamma))^6 + (2\alpha^3r_p^3+21\alpha^2\gamma r_p^3+6\alpha\gamma^2r_p^3+\gamma(27(r_i+\tau^0)^3-2\gamma^2r_p^3)^2))}\right)^{\frac{1}{3}}} +$$

$$\left. 2^{\frac{1}{3}}\left(2\alpha^3\gamma^3r_p^3 + 27\gamma^4(r_i+\tau^0)^3 + 21\alpha^2\gamma^4r_p^3 + 6\alpha\gamma^5r_p^3 - 2\gamma^6r_p^3 + \sqrt{(\gamma^6(-4r_p^6(\alpha-\gamma))^6 + (2\alpha^3r_p^3+21\alpha^2\gamma r_p^3+6\alpha\gamma^2r_p^3+\gamma(27(r_i+\tau^0)^3-2\gamma^2r_p^3)^2))}\right)^{\frac{1}{3}} \right)$$

References

Acocella, V., Mulugeta, G., 2001. Surface deformation induced by pluton emplacement: the case of Amiata (Italy). Physics and Chemistry of the Earth (A) 26, 355–362.

Albertz, M., Paterson, S.R., Okaya, D., 2002. Strain rates during pluton emplacement: extremely rapid host rock deformation or aureole displacement at background strain rates? Eos (Transactions of the American Geophysical Union), Fall Meeting Supplement 83, Abstract T51A–1122.

Benn, K., Odonne, F., de Saint-Blanquat, M., 1998. Pluton emplacement during transpression in brittle crust: new views from analogue experiments. Geology 26, 1079–1082.

Bons, P.D., Cox, S.J.D., 1994. Analogue experiments and numerical modeling on the relation between microgeometry and flow properties of polyphase materials. Materials Science and Engineering A175, 237–245.

Brown, E.H., McClelland, W.C., 2000. Pluton emplacement by sheeting and vertical ballooning in part of the southeast Coast Plutonic Complex, British Columbia. Geological Society of America Bulletin 112, 708–719.

Bruce, P.M., Huppert, H.E., 1990. Solidification and melting along dykes by the laminar flow of basaltic magma. In: Ryan, M.P., (Ed.), Magma Transport and Storage, pp. 87–101.

Brun, J.P., Gapais, D., Cogne, J.P., Ledru, P., Vigneresse, J.-L., 1990. The Flamanville granite (northwest France): an unequivocal example of a syntectonically expanding pluton. Geological Journal 25, 271–286.

Buddington, A.F., 1959. Granite emplacement with special reference to North America. Geological Society of America Bulletin 70, 671–747.

Clemens, J.D., 1998. Observations on the origins and ascent mechanisms of granitic magmas. Journal of the Geological Society, London 155, 843–851.

Clemens, J.D., Mawer, C.K., 1992. Granitic magma transport by fracture propagation. Tectonophysics 204, 339–360.

Clemens, J.D., Petford, N., 1999. Granitic melt viscosity and silicic magma dynamics in contrasting tectonic settings. Journal of the Geological Society, London 156, 1057–1060.

Clemens, J.D., Petford, N., Mawer, C.K., 1997. Ascent mechanisms of granitic magmas: causes and consequences. In: Holness, M.B., (Ed.), Deformation-enhanced Fluid Transport in the Earth's Crust and Mantle, pp. 144–171.

Corry, C.E., 1988. Laccoliths: mechanics of emplacement and growth. Geological Society of America Special Paper 220, 110pp.

Cruden, A.R., 1998. On the emplacement of tabular granites. Journal of the Geological Society, London 155, 853–862.

Cruden, A.R., McCaffrey, K.J.W., 2001. Growth of plutons by floor subsidence: implications for rates of emplacement, intrusion spacing, and melt-extraction mechanisms. Physics and Chemistry of the Earth (A) 26, 303–315.

Dunlap, W.J., Hirth, G., Teyssier, C., 1997. Thermomechanical evolution of a ductile duplex. Tectonics 16, 983–1000.

Fernandez, C., Castro, A., 1999. Pluton accommodation at high strain rates in the upper continental crust. The example of the Central Extremadura batholith, Spain. Journal of Structural Geology 21, 1143–1149.

Ferre, E., Glezizes, G., Bouchez, J.-L., Nnabo, P.N., 1995. Internal fabric and strike-slip emplacement of the Pan-African granite of the Solli Hills, northern Nigeria. Tectonics 14, 1205–1219.

Foster, D.A., Gray, D.R., 1999. Deformation rates and timing of deformation in the western Lachlan orogen, eastern Australia. Geological Society of America Abstracts with Program 31, 301.

Goodwin, L.B., Tikoff, B., 2002. Competency contrast, kinematics, and the development of foliations and lineations in the crust. Journal of Structural Geology 24, 1065–1085.

Guineberteau, B., Bouchez, J.-L., Vigneresse, J.-L., 1987. The Mortagne granite pluton (France) emplaced by pull-apart along a shear zone: structural and gravimetric arguments and regional implications. Geological Society of America Bulletin 99, 763–770.

Handy, M.R., Mulch, A., Rosenau, M., Rosenberg, C.L., 2001. The role of fault zones and melts as agents of weakening, hardening and differentiation of the continental crust: a synthesis. In: Holdsworth, R.E., Strachan, R.A., Magloughlin, J.F.,Knipe, R.J. (Eds.), The Nature and Tectonic Significance of Fault Zone Weakening. Geological Society of London Special Publication 186, pp. 305–332.

Hey, R.N., Johnson, P.D., Martinez, F., Korenaga, J., Somers, M.L., Huggett, Q.J., LeBas, T.P., Rusby, R.I., Naar, D.F., 1995. Plate boundary reorganization at a large-offset, rapidly propagating rift. Nature 378, 167–170.

Holder, M.T., 1979. An emplacement mechanism for post-tectonic granites and its implications for theri geochemical features. In: Atherton, M.P., Tarney, J. (Eds.), Origin of Granite Batholiths—Geochemical Evidence, pp. 116–128.

Hutton, D.H.W., 1982. A tectonic model for the emplacement of the main Donegal granite. Journal of the Geological Society, London 139, 615–631.

Hutton, D.H.W., 1988a. Granite emplacement mechanisms and tectonic

controls: inferences from deformation studies. Transactions of the Royal Society of Edinburgh, Earth Sciences 79, 245–255.

Hutton, D.H.W., 1988b. Igneous emplacement in a shear zone termination: the biotite granite at Strontian, Scotland. Geological Society of America Bulletin 100, 1392–1399.

Ji, S., Xia, B., 2002. Rheology of Polyphase Earth Materials, Polytechnic International Press, Montréal.

Johnson, S.E., Paterson, S.R., Tate, M.C., 1999. Structure and emplacement history of a multiple-center, cone-sheet-bearing ring complex: the Zarza Intrusive Complex, Baja California, México. Geological Society of America Bulletin 111, 607–619.

Johnson, S.E., Albertz, M., Paterson, S.R., 2001. Growth rates of dike-fed plutons: are they compatible with observations in the middle and upper crust? Geology 29, 727–730.

Johnson, S.E., Fletcher, J.M., Fanning, C.M., Vernon, R.H., Paterson, S.R., Tate, M.C., 2003. Structure, emplacement and in-situ expansion of the San José tonalite pluton, Peninsular Ranges batholith, Baja California, México. Journal of Structural Geology, 25(11), 1933–1957.

Johnson, S.E., Vernon, R.H., Upton, P., 2003b. Initiation of microshear zones and progressive strain-rate partitioning in the crystallizing carapace of a tonalite pluton: microstructural evidence and numerical modeling. Journal of Structural Geology 14, in press.

Knipe, R.J., 1989. Deformation mechanisms—recognition from natural tectonites. Journal of Structural Geology 11, 127–146.

Marsh, B.D., 1989. Magma chambers. Annual Reviews in Earth and Planetary Sciences 17, 439–474.

McCaffrey, K.J.W., Petford, N., 1997. Are granitic intrusions scale invarient? Journal of the Geological Society. London 154, 1–4.

Miller, R.B., Paterson, S.R., 1999. In defense of magmatic diapirs. Journal of Structural Geology 21, 1161–1173.

Molyneux, S.J., Hutton, D.H.W., 2000. Evidence for significant granite space creation by the ballooning mechanism: the example of the Ardara pluton, Ireland. Geological Society of America Bulletin 112, 1543–1558.

Morgan, S.S., Law, R.D., Nyman, M.W., 1998. Laccolith-like emplacement model for the Papoose Flat pluton based on porphyroblast-matrix analysis. Geological Society of America Bulletin 110, 96–110.

Muller, W., Aerden, D., Halliday, A.N., 2000. Isotopic dating of strain fringe increments: duration and rates of deformation in shear zones. Science 288, 2195–2198.

Nyman, M.W., Law, R.D., Morgan, S.S., 1995. Conditions of contact metamorphism, Papoose Flat Pluton, eastern California, USA: implications for cooling and strain histories. Journal of Metamorphic Geology 13, 627–643.

Paterson, S.R., Fowler, T.K., 1993. Re-examining pluton emplacement processes. Journal of Structural Geology 15, 191–206.

Paterson, S.R., Tobisch, O.T., 1992. Rates of processes in magmatic arcs: implications for the timing and mature of pluton emplacement and wall rock deformation. Journal of Structural Geology 14, 291–300.

Paterson, S.R., Fowler, T.K., Miller, R.B., 1996. Pluton emplacement in arcs: a crustal-scale exchange process. Transactions of the Royal Society of Edinburgh: Earth Sciences 87, 115–123.

Petford, N., 1996. Dykes or diapirs? Transactions of the Royal Society of Edinburgh: Earth Sciences 87, 105–114.

Petford, N., Kerr, R.C., Lister, J.R., 1993. Dike transport of granitoid magmas. Geology 21, 845–848.

Petford, N., Cruden, A.R., McCaffrey, K.J.W., Vigneresse, J.-L., 2000. Granite magma formation, transport and emplacement in the Earth's crust. Nature 408, 669–673.

Pfiffner, O.A., Ramsay, J.G., 1982. Constraints on geological strain rates: arguments from finite strain states of naturally deformed rocks. Journal of Geophysical Research 87, 311–321.

Prior, D.J., Knipe, R.J., Handy, M.R., 1990. Estimates of the rates of microstructural changes in mylonites. In: Knipe, R.J., Rutter, E.H. (Eds.), Deformation Mechanisms, Rheology and Tectonics. Geological Society of America Special Publication 54, pp. 309–319.

Ramsay, J.G., 1989. Emplacement kinematics of a grainite diapir: the Chindamora batholith, Zimbabwe. Journal of Structural Geology 11, 191–209.

Rubin, A.M., 1995. Getting granitic dikes out of the source region. Journal of Geophysical Research 100, 5911–5929.

de Saint-Blanquat, M., Law, R.D., Bouchez, J.-L., Morgan, S.S., 2001. Internal structure and emplacement of the Papoose Flat pluton: an integrated structural, petrographic, and magnetic susceptability study. Geological Society of America Bulletin 113, 976–995.

Schmid, S.M., 1989. Episodes in Alpine orogeny. Geological Society of America Abstracts with Program 21, 28.

Tikoff, B., Teyssier, C., 1992. Crustal-scale, en echelon 'P-shear' tensional bridges: a possible solution to the batholithic room problem. Geology 20, 927–930.

Tikoff, B., de Saint-Blanquat, M., Teyssier, C., 1999. Translation and the resolution of the pluton space problem. Journal of Structural Geology 21, 1109–1117.

White, J.C., Mawer, C.K., 1992. Deep-crustal deformation textures along megathrusts from Newfoundland and Ontario: implications for microstructural preservation, strain rates, and strength of the lithosphere. Canadian Journal of Earth Sciences 29, 328–337.

Wiebe, R.A., Collins, W.J., 1998. Depositional features and stratigraphic sections in granitic plutons; implications for the emplacement and crystallization of granitic magma. Journal of Structural Geology 20, 1273–1289.

Yoshinobu, A.S., Girty, G.H., 1999. Measuring host rock volume changes during magma emplacement. Journal of Structural Geology 21, 111–116.

Yoshinobu, A.S., Okaya, D.A., Paterson, S.R., 1998. Modeling the thermal evolution of fault-controlled magma emplacement models: implications for the solidification of granitoid plutons. Journal of Structural Geology 20, 1205–1218.